Observation of Surface/Defect States of SnO$_2$ Nanowires on Different Substrates from X-ray Excited Optical Luminescence

Dongniu Wang,[†,‡] Jinli Yang,[†] Xifei Li,[†] Jiajun Wang,[†] Ruying Li,[†] Mei Cai,[§] T. K. Sham,*[,‡] and Xueliang Sun*[,†]

[†]Department of Mechanical and Materials Engineering, University of Western Ontario, London N6A 3K7, Ontario, Canada
[‡]Depeartment of Chemistry, University of Western Ontario, London N6A 3K7, Ontario, Canada
[§]General Motors R&D Center, Warren, Michigan 48090-9055, United States

S Supporting Information

ABSTRACT: SnO$_2$ nanowires (NWs) have been successfully synthesized on two different substrates (stainless steel (SS) and copper) via a facile hydrothermal process. SnO$_2$ NWs with varying degrees of crystallinity are obtained on different substrates. The growth mechanisms are also deducted by observing the morphology revolution at various reaction times. Furthermore, the electronic structures and optical properties have been investigated by X-ray absorption near edge structure (XANES) and X-ray excited optical luminescence (XEOL) measurements. The yellow-green luminescence from SnO$_2$ NWs is originated from the intrinsic surface states. Compared with SnO$_2$ NWs on copper, a near infrared (NIR) luminescence is observed for SnO$_2$ NWs on SS, which resulted from poor crystallinity and an abundance of defect/surface states.
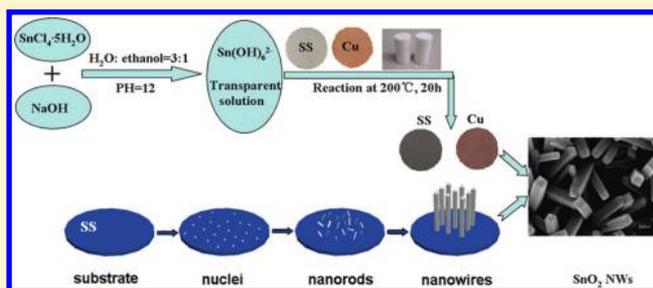
1. INTRODUCTION

Tin dioxide (SnO$_2$), an n-type semiconductor material with a wide band gap of ~3.6 eV (room termperature), has been widely exploited due to its distinct optical and electrical properties. Many advantages such as high optical transparency and chemical sensitivity, have made it an attractive material for a wide variety of applications in solar cells,[1] field effect transistors,[2,3] catalyst support for fuel cells,[4,5] sensors,[6–8] and Li-ion batteries.[9–12] Recently, nanomaterials especially one-dimensional SnO$_2$ nanostructures have been applied in various advanced electric systems owing to their superior electrochemical,[13,14] catalytic,[4,5] and optical properties[15,16] compared with those of bulk SnO$_2$.

For the preparation of one-dimensional SnO$_2$ nanostructure on substrates, the methodology can be mainly divided into two categories: vapor phase growth and solution phase growth. The vapor phase technique is well-developed based on the reaction between tin vapor and oxygen gas.[17–21] Although high purity and high quality SnO$_2$ NWs can be synthesized on various substrates, critical conditions, such as high temperature and the presence of a catalyst, are required, not to mention the low yield and high cost which limit its large-scale production. However, solution-phase growth methods provide a more flexible control and can be done at lower cost. To obtain one-dimensional SnO$_2$ structure with controlled diameter and length with solution phase growth, many templates such as anodic aluminum oxide, molecular sieves, and polymer membranes have been used.[22,23] However, these methods generally require fussy multiple steps and specific templates,

which make it a time-consuming process with accompanying high cost. For template-free methods, organic solvents[24,25] are generally used, which are deleterious to the environment. In addition, removing the surfactant after the reaction can make the synthesis very cumbersome. Recently, a one-step hydrothermal process[26–31] was demonstrated to be desirable for the synthesis of SnO$_2$ NW arrays directly on metallic current collector substrates. Because of the environment friendly solvent (usually water and ethanol), the surfactant free process, and the lack of need of a catalyst, a pure product can be developed by this process. But up to date, despite these findings, there is no report elucidating the growth mechanism of SnO$_2$ nanowire on a substrate, especially the effect of substrates on the evolution of SnO$_2$ morphology.

Applying a substrate could introduce an interface between the products and the substrate. Because of the various types and degrees of strains originated from the lattice mismatch between products and substrates, the crystal growth behavior on different substrates is strongly affected,[32,33] leading to different densities of surface or defect states.[34,35] As previously reported, the surface and defect states play a crucial role in the luminescence.[36,37] However, the relationship between the density of the defect state and luminescence is still unclear.

XANES is a spectroscopic technique that can characterize electronic structures by measuring the X-ray absorption

Scheme 1. Synthetic Drawing of the Preparation of SnO$_2$ NWs on Substrates
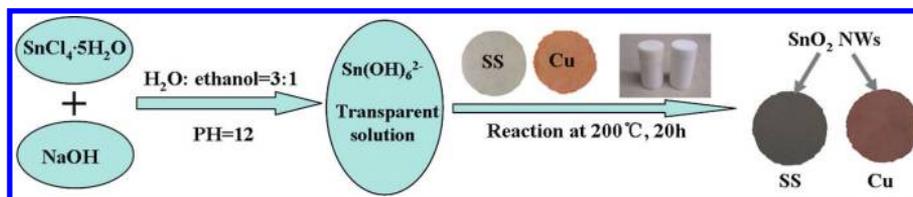
coefficient of an element of interest in the material. XANES arises from the dipole excitation of a core electron into previously unoccupied electronic states in the valence region and beyond. Since valence states are chemically sensitive, XANES probes the local chemistry (population and symmetry of unoccupied electronic states, e.g., LUMO in molecules and the conduction band in semiconductors) of the absorbing atom. Using a tunable synchrotron light source, one can probe the local symmetry and occupation (densities of states) of these states including surface and defect states by tracking the absorption coefficient of the element of interest by scanning the photon energy across the absorption edge, e.g., the Sn M$_{5,4}$ edge and O K-edge in the case of this study. XEOL, an X-ray photon in the optical photon out technique is used to monitor the optical luminescence (UV−visible-Near IR) at selected excitation photon energies, often across the absorption edge; this technique can provide element and site specificity under favorable conditions, and one then can determine the origin of the luminescence observation.

In this article, we choose two typical substrates to grow SnO$_2$ nanostructures and systematically study the formation mechanism. This study reveals the significant effects of surface or defect states on luminescence using synchrotron light source based XANES and XEOL techniques.

2. EXPERIMENTAL SECTION

Synthesis SnO$_2$ NWs on Different Substrates. In a typical experiment to grow SnO$_2$ on stainless steel (SS 304 L), 350.58 mg of SnCl$_4$·5H$_2$O (1 mmol) and 700 mg of NaOH (17.5 mmol) were dissolved in a mixture of a 40 mL of water/ethanol (1:3) solution. To conduct the synthesis, the alkaline PH value around 12 was needed. After sonication and continuous stirring for about 10 min, a transparent solution was obtained. Then 10 mL of the solution was transferred to a Telfon-lined autoclave (20 mL) where the substrate, cleaned by acetone beforehand, was laid flat at the bottom of the autoclave. The solution was subsequently heated to 200 °C at a rate of 5 °C per min from room temperature, then maintained for 20 h, and then cooled down to room temperature. Once the reaction was completed, the SnO$_2$ covered substrate was rinsed several times with distilled water and ethanol, followed by final drying at 60 °C overnight. Similar procedures were used for SnO$_2$ NWs grown on copper foil. After the alkaline hydrothermal process, both of the substrates' surfaces were covered with white-gray products. A schematic representation for the preparation of SnO$_2$ NWs is given in Scheme 1.

Characterization. The morphology and phase composition were characterized and analyzed by powder X-ray diffraction (XRD, Rigaku RU-200BVH) with Co Kα radiation (λ = 0.179 nm), on a field-emission scanning electron microscope (FESEM, Hitachi S-4800, operating at 5 kV) equipped with an energy-dispersive X-ray spectrometer (EDX). The XANES and XEOL experiments were conducted on the undulator Spherical Grating Monochromator (SGM) beamline at the Canadian Light Source (CLS) located at the University of Saskatchewan in Saskatoon. The SGM beamline employs three diffraction gratings to provide a very bright, highly mono-chromatic photon beam ($E/\Delta E$ ~10,000), tunable between 250 and 2000 eV.[38] XEOL was recorded with an Ocean Optics, QE65000 spectrometer, which is equipped with a dispersive grating and a CCD

detector collecting all wavelengths (200 −900 nm) simultaneously at any given excitation energy.

3. RESULTS AND DISCUSSION

Morphology and Structures. Figure 1a and b shows the typical SEM images, top view and side view respectively, of the
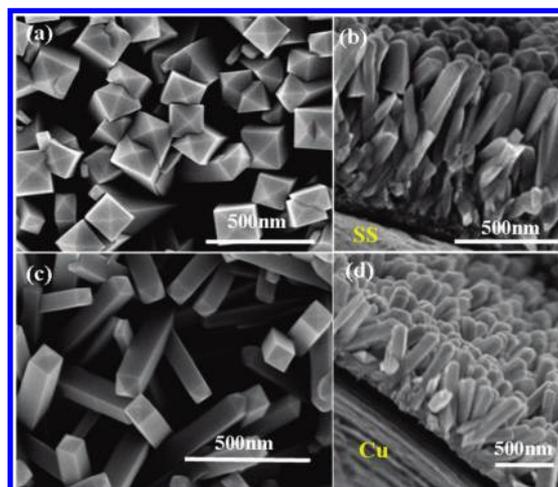

Figure 1. SEM images of SnO$_2$ NWs growing on different substrates: stainless steel, (a) top view and (b) side view; copper as substrate, (c) top view and (d) side view.

as synthesized SnO$_2$ NW arrays vertically grown on SS. It can be seen that the NWs were uniformly distributed on the substrate, with a diameter from 100−150 nm and a length around 500 nm with an octahedral tip. Compared with SnO$_2$ NWs grown on SS, SnO$_2$ NWs on copper have similar shape, with the same octahedral structure tip, length, and diameter, but are grown in a more random manner as illustrated in Figure 1c and d.

Morphology Evolution. To study the growth mechanism, a different reaction time was chosen to investigate the morphology evolution of SnO$_2$ NWs on SS. Figure 2a shows a series of typical morphologies from short reaction time (5 h) to aim-reaction time (20 h) during hydrothermal synthesis. It can be clearly seen that there exists a morphology trans-formation from initial nuclei of the sharp tip (5 h), to small aggregates consisting of an irregular needle-like structure (10 h), and to NW structure with the octahedral tip (15 h), until all precursors transform to SnO$_2$ NW arrays (20 h). With increase of the reaction time, the density of SnO$_2$ NWs increases, and finally, SnO$_2$ NWs vertically grow on the substrate after 20 h. A similar morphology evolution for SnO$_2$ NWs on copper foil was also observed in Figure S1 (see Supporting Information). Because of different surface roughness, the growth direction to SnO$_2$ on copper is not as vertical as that of SnO$_2$ on SS, as one can infer from the initial steps on the copper substrate.
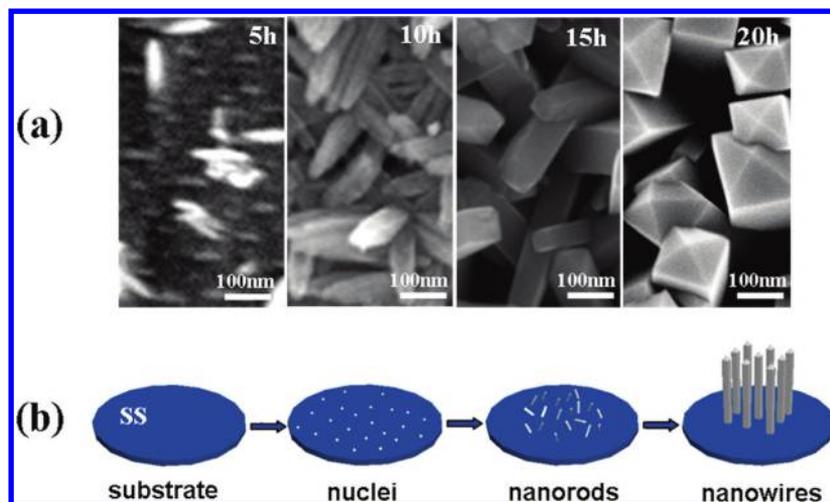
Figure 2. (a) morphology evolution of SnO$_2$ NWs on SS at different reaction time; (b) schematic SnO$_2$ NW growth mechanism.

As previously reported,[25] the energy barrier between (001) and the other facets were leveled by the excessive thermal energy supplied to the system. The scheme for a proposed possible growth mechanism is presented in Figure 2b.The hydrolysis of saturated Sn(OH)$_6^{2-}$ forms the SnO$_2$ nuclei (see following equations) on the substrates at first; it is worth mentioning that the SnO$_2$ nuclei could not form unless the substrate is present in the solution, that is, the substrate could faciliate the formation of SnO$_2$ nuclei, then due to the hydrothermal condition, the kinetics controls the SnO$_2$ anisotropic growth to facilitate the [001] direction growth; thus, the SnO$_2$ NWs arrays are obtained on the metallic substrates. With time, both the diameter and the length of the nanorod increase on the substrate, and the sample on SS is more ordered than copper due to the surface difference (Cu is more susceptible to roughening than SS).
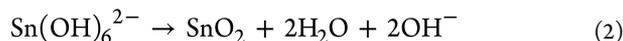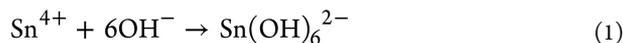
$$Sn^{4+} + 6OH^- \rightarrow Sn(OH)_6^{2-} \tag{1}$$

$$Sn(OH)_6^{2-} \rightarrow SnO_2 + 2H_2O + 2OH^- \tag{2}$$

Figure 3 compares the XRD patterns of these samples. It can be seen that except for the peaks originating from the
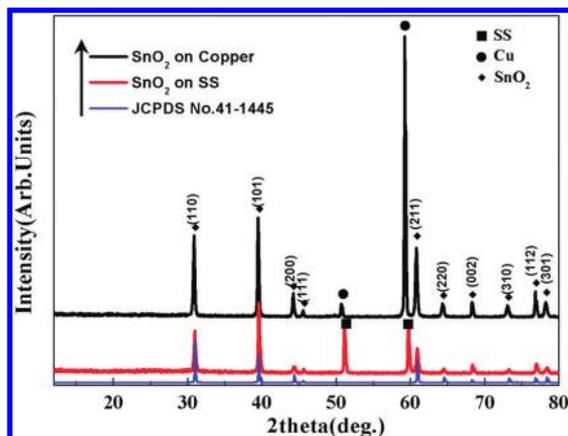

Figure 3. XRD patterns of as prepared SnO$_2$ NWs grown on SS and copper substrates.

substrates, all other peaks arise from the SnO$_2$ rutile structure (JCPDS no. 41-1445). For these samples, the strongest peak

corresponds to the (101) plane, demonstrating that individual SnO$_2$ nanostructures are crystallized along the *c*-axis. For SnO$_2$ grown on SS and copper, the ratio of faces between (002)/(101) is higher than those of reference values for crystalline SnO$_2$ (JCPDS no. 41-1445), indicating that individual SnO$_2$ nanostructures are crystallized along the (001) direction. It is worth mentioning that although both samples are crystallized SnO$_2$, the peaks for SnO$_2$ grown on SS are not as strong as that on copper, which means that it is less crystalline or richer in surface or defect states. Compared with Huang's work,[30,31] where SnO$_2$ nanoarrays were fabricated vertically on Ni, Ti, and Fe−Co−Ni substrates without comparing degrees of crystallinity, here, we reveal that different substrates could affect the quality of crystallinity of SnO$_2$ they supported. Similar to Ghosh's study[32] that the structure of ZnO is affected by different substrates, in this study, SS and copper have significantly different lattice parameters, and the lattice mismatch between SS and SnO$_2$ is more serious than that between copper and SnO$_2$, resulting in a bigger strain at the interface, which favors the creation of higher disorder SnO$_2$ crystallites.

Electronic and Optical Properties (XANES and XEOL). The intriguing surface and defect related optical properties have prompted us to exploit the unusual electronic properties exhibited by SnO$_2$ nanowires when they are employed on the nanoscale since this behavior is not well understood. In order to better understand the unusual phenomena, we must have a better understanding of the electronic structure of SnO$_2$ nanostructures. To this end, we have conducted X-ray absorption near edge structure (XANES) and X-ray excited optical luminescence measurement (XEOL) using synchrotron radiation on these SnO$_2$ nanowires prepared on different substrates to study more about the electronic structure and optical properties of these SnO$_2$ nanowires.

Figure 4 shows the XANES spectra for SnO$_2$ NWs grown on different substrates measured in total electron yield (TEY), fluorescence yield (FLY), and photoluminescence yield (PLY). In the Sn M$_{5,4}$ edge XANES (Figure 4a and c), two sets of triplet peaks begin at ~490 and 498 eV, corresponding to 3d$_{5/2}$ and 3d$_{3/2}$ to 5p transitions, respectively. These features are characteristic of the SnO$_2$ nanostructure (rutile) as reported previously.[36] The Sn M$_{5,4}$ edge tracked by the three yields (TEY, FLY, and PLY) are similar, i.e., that all exhibit positive
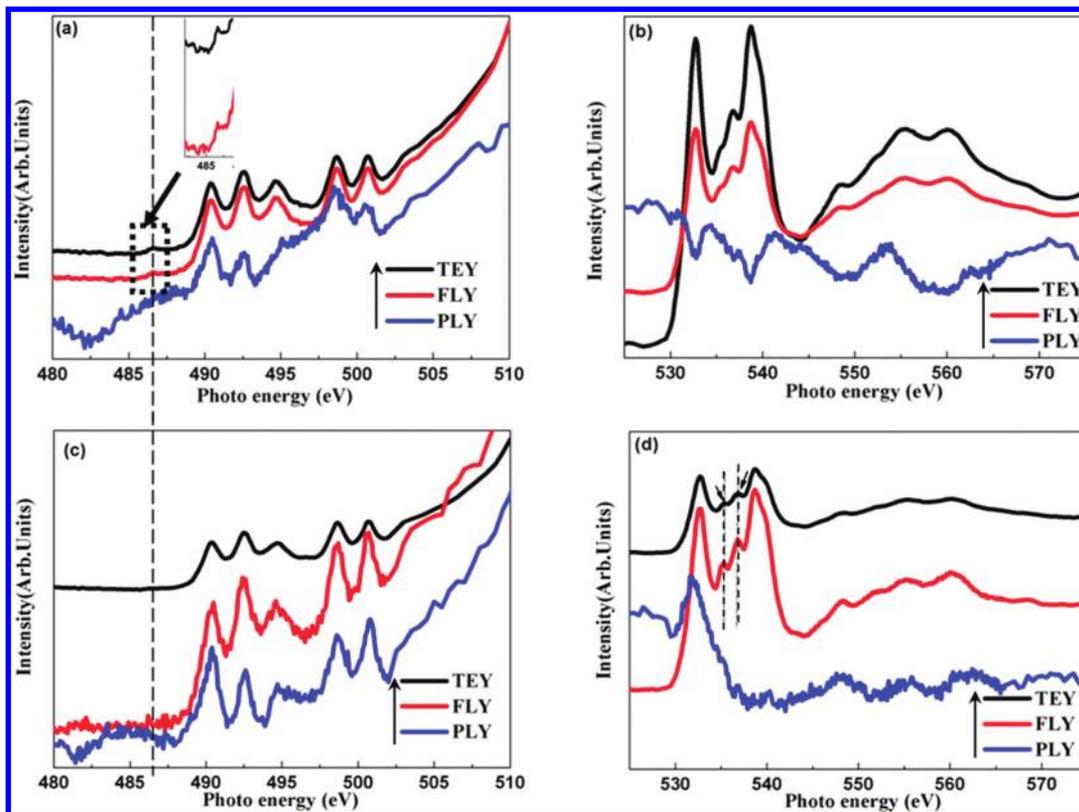
Figure 4. O K-edge and Sn M$_{5,4}$ edge XANES spectra of SnO$_2$ NWs grown on SS (a) Sn M$_{5,4}$ edge and (b) O K-edge, on copper (c) Sn M$_{5,4}$ edge, and (d) O K-edge.
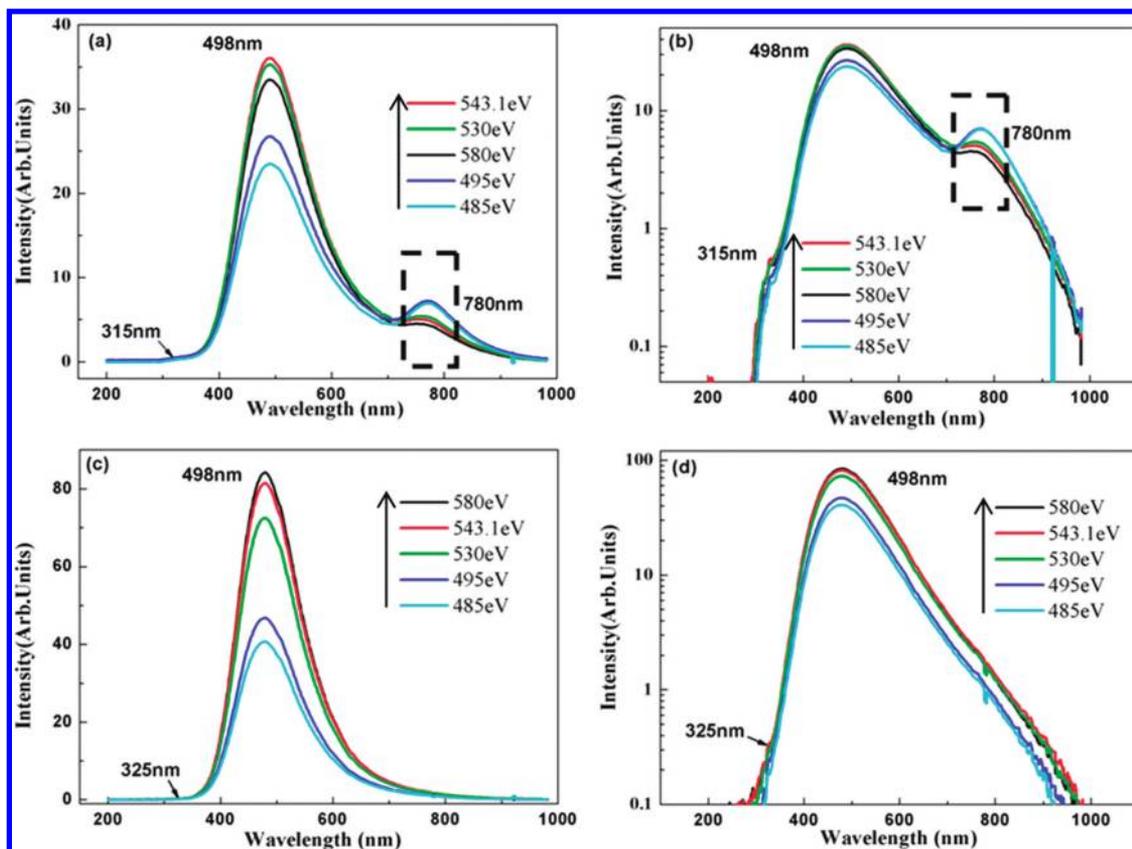

Figure 5. XEOL of SnO$_2$ NWs on different substrates: (a,b) SS; (c,d) copper.

edge jumps. For SnO$_2$ grown on SS, (see Figure 4a), the TEY and FLY spectra show a pre-edge resonance at 486.5 eV (clearly shown in enlarged spectra in the insert) just before the Sn M$_{5,4}$ edge, which has been previously attributed to surface states caused by unsaturated coordination of surface Sn ions due to oxygen vacancies.[37] This observation is confirmed by the very intense third peak of the first triplet (M$_5$) caused by contribution from the surface state for the M$_4$ edge underneath. For the copper substrate, the surface sensitive TEY and bulk sensitive FLY and optically sensitive PLY of the Sn M edge are also similar. It is noteworthy that there is no pre-edge resonance peak at 486.5 eV before the Sn M-edge for SnO$_2$ on copper substrate. Meanwhile, the third peak of the first triplet (M$_5$) is less intense compared to that of SS, indicating the defect/surface states are less abundant for SnO$_2$ on copper substrates which are in accordance with the XRD results. Further examination of the PLY spectrum in Figure 4a, reveals the pre-edge and the very intense third peak of the first triplet (M$_5$) (arrow pointed) in PLY indicating that the selective excitation of Sn associated with defects has a strong effect on the luminescence yield. For SnO$_2$ on the copper substrate, at the resonance, the PLY spectrum (figure 4b) shows a less intense peak which is due to the low densities of surface or defect states.

Turning to the O K-edge, it is found that the FLY XANES tracks that of TEY but that the PLY does not. In fact, the PLY is inverted; this inversion (reduction in quantum yield at the edge) is due to saturation (self-absorption) effect. A simple calculation using the X-ray calculator (http://henke.lbl.gov/optical_constants/atten2.html) shows that for SnO$_2$, the attenuation length of the incident photon is considerable longer (at least a factor of 3) at the SnM$_{5,4}$ edge than at the O K-edge. Thus, in a total absorption situation, as is in the case of most soft X-ray absorption measurements of solids, the penetration depth of the photon at the O K-edge is significant shorter than that at the Sn M$_{5,4}$ edge. Since the secondary process (attenuation of energetic electrons and fluorescent X-rays describe above) contributes significantly in the energy transfer to the optical de-excitation channel, a reduction in the secondary events will reduce the photoluminescence. Thus, the photoelectrons, Auger electron, and fluorescence X-rays associated with the O 1s core hole will have a good chance of escaping the surface without contributing to the secondary processes (thermalization of electrons and holes), which in turn contribute to the photoluminescence, resulting in a negative edge jump when the absorption coefficient increases sharply at the edge threshold. In other words, above the O K-edge, the optical photons produced per eV of energy absorbed are less than that just below the edge. The crystallinity could also be deducted from O K-edge spectra. Closer examination of the O K-edge TEY XANES reveals that the spectral feature for SnO$_2$ on copper is sharper than SS (as marked by lines and arrows), indicating higher quality crystallites of SnO$_2$ NWs on copper (less disorder or surface and defects states). This conclusion also proves the point that degrees of crystallinity for SnO$_2$ rely on the substrate we mentioned above.

In order to investigate the luminescence properties of SnO$_2$ NWs with different densities of surface or defects states, XEOL was performed at room temperature, as shown in Figure 5. Each sample was excited with soft X-ray photons both below and above the threshold of the O K-edge and Sn M$_{5,4}$-edge. This is equivalent to the XEOL excited using selected excitation energy in the PLY XANES shown above. All spectra show an

intense emission band from 400 to 900 nm (3.1−1.4 eV), centered on 498 nm (yellow-green luminescence) which has been reported in XEOL studies of SnO$_2$ nanoribbons originating from intrinsic surface states.[36,37] Very weak emission was observed originating from the band gap of SnO$_2$ (3.6 eV), which would have resulted in a peak at 344 nm. It has been shown previously that near band gap emission is quenched by the surface or defect states in the band gap of SnO$_2$. A log plot of the XEOL does show a weak band gap feature. For SS, it can be seen in the XEOL spectra that the luminescence intensity increases across the Sn M$_{5,4}$ edge but that the intensity decreases across the O K-edge as displayed above in the PLY-XANES.

For SnO$_2$ grown on the SS substrate, which is less crystalline, two distinct features are observed, as compared to the XEOL from crystalline SnO$_2$ on copper; first, the short wavelength onset exhibits a more pronounced feature at 315 nm (∼3.9 eV) as compared to 325 nm (∼3.8 eV), indicating that the band gap widens much due to quantum confinement. More importantly, SnO$_2$ on SS exhibits a near IR peak at 780 nm (1.6 eV), resulting from the high density of surface or defect states, which is totally absent in SnO$_2$ on copper (as marked by the frame). From the XEOL, together with the PLY data, it can be seen that for SnO$_2$ on SS when excited at 485 eV and 495 eV (Sn ion associated with defects), the transition from Sn 3d$_{5/2}$ to surface or defect states is turned on, and the intensity of luminescence at 780 nm increases markedly compared with those with off-resonance excitations, e.g., at 530 eV, 543.1 eV, and 580 eV. This observation indicates that the near IR peak 780 nm (1.6 eV) results from high densities of surface or defect states. Thus, the high density of surface or defect states affects bands of the SnO$_2$ NWs, then inducing the near IR luminescence. Incidentally, a similar IR band is observed in the rutile structure of the TiO$_2$ nanotube, a somewhat stressed structure.[39] More studies are required to identify the origin of this emission for certainty.

CONCLUSIONS

In conclusion, vertically aligned SnO$_2$ NWs arrays are obtained on SS and copper substrates via the hydrothermal route. The NWs have a diameter from 100 to 150 nm and a length around 500 nm with an octahedral tip. For the copper substrate, random oriented SnO$_2$ NWs were formed after the 20 h reaction. Morphology evolution explains the growth mechanism, from initial nuclei to SnO$_2$ NW arrays. XEOL data shows that both SnO$_2$ samples exhibit yellow-green luminescence, which originates from the intrinsic surface states. Moreover, SnO$_2$ NWs on SS have lower quality of crystallites with more defect/surface states than that of copper ones as proved by XRD and XANES. It is noteworthy that SnO$_2$ on SS showed unique near IR luminescence, which is attributed to high density of surface or defect states itself. From our measurement, luminescence depends on the degree of crystallinility of SnO$_2$, revealing that the bands of the semiconductor materials are related to the density of surface or defect states.

ASSOCIATED CONTENT

S Supporting Information

SEM images for morphologies of the evolution of SnO$_2$ NWs on copper at different reaction times. This material is available free of charge via the Internet at http://pubs.acs.org.

■ AUTHOR INFORMATION

Corresponding Author
*E-mail: tsham@uwo.ca (T.K.S.); xsun@uwo.ca (X.S.).

■ REFERENCES

(1) Chappel, S.; Chen, S. G.; Zaban, A. *Langmuir* **2002**, *18*, 3336−3342.

(2) Sun, J.; Tang, Q. X. *Nanotechnology* **2009**, *20*, 255202.

(3) Dattoli, E. N.; Wan, Q.; Guo, W.; Chen, Y.; Pan, X.; Lu, W. *Nano Lett.* **2007**, *7*, 2463−2469.

(4) Saha, M.; Li, R.; Cai, M.; Sun, X. *Electrochem. Solid-State Lett.* **2007**, *10*, B130−B133.

(5) Saha, M.; Li, R.; Sun, X. *Electrochem. Commun.* **2007**, *9*, 2229−2234.

(6) Wei, B. Y.; Hsu, M. C.; Su, P. G.; Lin, H. M.; Wu, R. J.; Lai, H. J. *Sens. Actuators, B* **2004**, *101*, 81−89.

(7) Liu, Y. L.; Yang, H. F.; Yang, Y.; Liu, Z. M.; Shen, G. L.; Yu, R. Q. *Thin Solid Films* **2006**, *497*, 355−360.

(8) Leite, E. R.; Weber, I. T.; Longo, E.; Varela, J. A. *Adv. Mater.* **2000**, *12*, 965−968.

(9) Courtney, I. A.; Dahn, J. R. *J. Electrochem. Soc.* **1997**, *144*, 2045−2052.

(10) Kim, D. W.; Hwang, I. S.; Kwon, S. J.; Kang, H. Y.; Park, K. S.; Choi, Y. J.; Choi, K. J.; Park, J. G. *Nano Lett.* **2007**, *7*, 3041−3045.

(11) Wang, Y.; Lee, J. Y. *J. Phys. Chem. B* **2004**, *108*, 17832−17837.

(12) Ying, Z.; Wan, Q.; Cao, H.; Song, Z. T.; Feng, S. L. *Appl. Phys. Lett.* **2005**, *87*, 113108.

(13) Park, M. S.; Wang, G. X.; Kang, Y. M.; Wexler, D.; Dou, S. X.; Liu, H. K. *Angew. Chem., Int. Ed.* **2007**, *46*, 750−753.

(14) Wang, Y.; Zeng, H. C.; Lee, J. Y. *Adv. Mater.* **2006**, *18*, 645−649.

(15) Hu, J. Q.; Bando, Y.; Liu, Q. L.; Golberg, D. *Adv. Funct. Mater.* **2003**, *13*, 493−496.

(16) Fan, W. Q.; Song, S. Y.; Feng, J.; Lei, Y. Q.; Zheng, G. L.; Zhang, H. J. *J. Phys. Chem.C* **2008**, *112*, 19939−19944.

(17) Lu, J. G.; Chang, P. C. *Mater. Sci. Eng., R* **2006**, *52*, 49−91.

(18) Ying, Z.; Wan, Q. *Nanotechnology* **2004**, *15*, 1682−1684.

(19) Ahn, J. H.; Kim, Y. J.; Wang, G. X. *J. Alloy. Compd.* **2009**, *483*, 422−424.

(20) Ko, Y. D.; Kang, J. G. *Nanotechnology* **2009**, *20*, 455701.

(21) Mathur, S.; Barth, S. *Small* **2007**, *3*, 2070−2075.

(22) Zhao, N. H.; Yang, L. C.; Zhang, P.; Wang, G. J.; Wang, B.; Yao, B. D.; Wu, Y. P. *Mater. Lett.* **2010**, *64*, 972−975.

(23) Kim, H.; Cho, J. *J. Mater. Chem.* **2008**, *18*, 771−775.

(24) Wang, Y.; Jiang, X.; Xia, Y. *J. Am. Chem. Soc.* **2003**, *125*, 16176−16177.

(25) Zhang, D. F.; Sun, L. D.; Xu, G.; Yan, C. H. *Phys. Chem. Chem. Phys.* **2006**, *8*, 4874−4880.

(26) Shi, S. L.; Liu, Y. G. *Chin. Phys. B* **2009**, *18*, 1674−1056.

(27) Qin, L. P.; Xu, J. Q.; Dong, X. W.; Pan, Q. Y.; Cheng, Z. X.; Xiang, Q.; Li, F. *Nanotechnology* **2008**, *19*, 185705.

(28) Cheng, B.; Russell, J. M.; Shi, W. S.; Zhang, L.; Samulski, E. T. *J. Am. Chem. Soc.* **2004**, *126*, 5972−5973.

(29) Ye, J. F.; Qi, L. M. *J. Mater. Sci. Technol.* **2008**, *24*, 529−540.

(30) Ji, X. X.; Huang, X. T. *Nanoscale Res. Lett.* **2010**, *5*, 649−653.

(31) Liu, J. P.; Li, Y. Y.; Huang, X. T.; Ding, R. M.; Hu, Y. Y.; Jiang, J.; Liao, L. *J. Mater. Chem.* **2009**, *19*, 1859−1864.

(32) Ghosh, R.; Basak, D.; Fujihara, S. *J. Appl. Phys.* **2004**, *96*, 2689.

(33) Schwenzer, B.; Gomm, J. R.; Morse, D. E. *Langmuir* **2006**, *22*, 9829−9831.

(34) Lee, H. Y.; Ko, H. J.; Yao, T. *Appl. Phys. Lett.* **2003**, *82*, 523.

(35) Shi, W. S.; Agyeman, O.; Xu, C. N. *J. Appl. Phys.* **2002**, *91*, 5640.

(36) Zhou, X. T.; Heigl, F.; Murphy, M. W.; Regier, T.; Coulthard, I.; Blyth, R. I. R.; Sham, T. K. *Appl. Phys. Lett.* **2006**, *89*, 213109.

(37) Zhou, X. T.; Zhou, J. G.; Murphy, M. W.; Ko, J. Y. P.; Heigl, F.; Regier, T.; Blyth, R. I. R.; Sham, T. K. *J. Chem. Phys.* **2008**, *128*, 144703.

(38) Regier, T.; Paulsen, J.; Wright, G.; Coulthard, I.; Tan, K. H.; Sham, T. K.; Blyth, R. I. R. *AIP Conf. Proc.* **2007**, *879*, 473−476.

(39) Liu, L. J.; Chen, J.; Sham, T. K. *J. Phys. Chem. C* **2010**, *114*, 21353−21359.